Distributions of Ionic Concentrations and Electric Field around the Three-Phase Contact at High Rates of Langmuir−Blodgett Deposition

M. P. Bondarenko,[†] E. K. Zholkovskiy,[†] V. I. Kovalchuk,[†] and D. Vollhardt*[,‡]

Institute of Biocolloid Chemistry of NAS of Ukraine, Vernadskogo, 42, 03142 Kiev, Ukraine and Max Planck Institute of Colloids and Interfaces, D-14424 Potsdam/Golm, Germany

Received: October 21, 2005; In Final Form: December 6, 2005

A mathematical problem is formulated and numerically solved for addressing the electric field and ionic concentration distributions developing around the three-phase contact line during the Langmuir−Blodgett deposition of charged monolayers. Compared to a previous paper dealing with the same effect (*J. Phys. Chem. B* **2004**, *108*, 13449), the present analysis is not restricted to the case of low deposition rates and small concentration changes. The obtained results show that, for sufficiently high deposition rates, the subphase composition substantially changes in the immediate vicinity of the three-phase contact line. It is shown that the predicted changes in the subphase composition can drastically affect the adhesion work and the dynamic contact angle. On this basis, the influence of the concentration polarization effect on meniscus behavior is discussed.

1. Introduction

In our previous studies, it was shown that during the Langmuir−Blodgett (LB) deposition of a monolayer, which is formed by dissociating amphiphile molecules, both ionic concentration profiles and an electric field are developed around the three-phase contact line in the subphase.[1−3] Using the analogy between this effect and similar effects observed in membrane systems, we denote the concentration profile formation as concentration polarization.[1−3] On the other hand, this effect has many things in common with nonequilibrium nonlinear electrokinetic phenomena[4,5] and can be investigated using standard methods proposed for such phenomena.

The concentration polarization effect occurs because the deposited film removes ions from the subphase meniscus region in another proportion than that defined by the ion convective fluxes through a cross-section of the meniscus region. The convective flux of an ion is determined by integrating the product of the local velocity and ion concentration over the cross-section area. Due to the liquid incompressibility, the above-mentioned integral takes a zero value when, within a meniscus area cross-section, an ion is distributed uniformly. When an ion is distributed nonuniformly, its convective flux through the cross-section takes a nonzero value. Such a nonuniformity in ionic distributions exists due to the presence of the diffuse electric double layers adjacent to the liquid−solid and gas−liquid interfaces.

In the presence of the double layer, the convective flux of counterions (coions) through the cross-section of the meniscus region is directed toward (outward) the three-phase contact line. Usually, the relationships between such convective fluxes differ from the relationship between the numbers of ions, which, per unit of time, are removed from the liquid by the deposited film. For example, the ions of an indifferent electrolyte are not removed by the deposited film at all. At the same time, due to the presence of the double layers, the ion convective fluxes through any cross-section take nonzero values.

Due the above-discussed misbalance, the purely convective fluxes cannot provide the steady-state conservation of ions. Consequently, to maintain the steady-state balance, the electromigration fluxes, the corresponding ion concentration, and electric potential profiles appear in the meniscus region. The developed concentration profiles depend on the substrate velocity. As a result, while withdrawing the substrate with a given velocity in the immediate vicinity of the three-phase contact line, the subphase composition becomes different from that in the equilibrium state (i.e., at zero substrate velocity). Such changes in the subphase composition can dramatically affect the meniscus behavior.

A possible mechanism, due to which the concentration polarization affects the meniscus behavior, can be associated with the concentration dependence of the unbalanced surface tension force, f, acting on the three-phase contact line upward. Assuming the three-phase contact line bears zero electric charge and considering small contact angles, such a force is given by an expression similar to that employed by de Gennes[6,7]

$$f = \gamma[\cos(\theta) - \cos(\theta_e)] \approx -\frac{\gamma}{2}(\theta^2 - \theta_e^2) \qquad (1)$$

The latter expression in eq 1 is valid for small angles. In eq 1, γ is the gas−liquid interfacial tension; θ is the dynamic contact angle; θ_e is the equilibrium contact angle that, for $\theta_e \ll 1$, is expressed as

$$\theta_e \approx (2W/\gamma)^{1/2} \qquad (2)$$

where W is the adhesion work.

Studying the influence of the subphase composition on the equilibrium contact angle, θ_e, different authors observed substantial changes in θ_e while varying the subphase pH within the range $2 < \mathrm{pH} < 8$. In the literature, this effect is explained by a strong dependency of the adhesion work, W, on the subphase pH.[8−10] At the same time, changes in W and γ with

* To whom correspondence should be addressed. E-mail: vollh@mpikg-golm.mpg.de.
† Institute of Biocolloid Chemistry of NAS of Ukraine.
‡ Max Planck Institute of Colloids and Interfaces.

10.1021/jp056042x CCC: $33.50
Published on Web 01/07/2006

pH, evaluated within the framework of the DLVO approach, seem to be insufficient for explaining the behavior of the equilibrium contact angle.[1,2,9] Therefore, different hypotheses have been proposed regarding a possible mechanism responsible for the strong dependency of the adhesion work on the subphase pH: formation of hydrogen bonds bridging the liquid−solid and gas−liquid interfaces,[9] ion correlation effects making the electrostatic force acting between the similarly charged interfaces to be attractive, etc.[11,12]

Details of the above-mentioned mechanism of variation of the adhesion work still remain unclear. However, the experimentally found fact of a strong dependence of the equilibrium contact angle on the subphase composition is extremely important for understanding the role of concentration polarization in the meniscus dynamics.

In the equilibrium state, both adhesion work and contact angle are functions of all ion concentrations in the immediate vicinity of the three-phase contact line, $C^*_{i(eq)}$, i.e., $W = W(C^*_{i(eq)})$ and $\theta = \theta_e(C^*_{i(eq)})$. Let us now consider the substrate withdrawal with a given speed U and assume that the interfacial quasi-equilibrium is established infinitely fast. For such a dynamic regime, the adhesion work and the contact angle remain the same functions of the ion concentrations in the immediate vicinity of the three-phase contact line, C^*_i, as those in the equilibrium state, $W = W(C^*_i)$ and $\theta = \theta_e(C^*_i)$. However, due to the concentration polarization effect, the dynamic concentration C^*_i differs from $C^*_{i(eq)}$and depends on the substrate speed, U, i.e., $C^*_i = C^*_i(U)$.

Thus, while accounting for the concentration polarization effect, the parameter θ_e in eq 1 becomes dependent on the substrate speed U. Consequently, the concentration polarization affects also the driving force f given by eq 1. Obtaining the driving force as a function of the substrate speed, $f(U)$, is an important element in the analysis of the meniscus dynamics.

Determining the function $f(U)$ can be decomposed in two stages. The first one is associated with the equilibrium analysis intended for obtaining the dependencies $W = W(C^*_{i(eq)})$ and/or $\theta = \theta_e(C^*_{i(eq)})$. For example, the latter functions can be extracted from experimental data. The second necessary stage amounts to evaluating the functions $C^*_i = C^*_i(U)$ that describe the variation of the ith ion concentration in the immediate vicinity of the three-phase contact line.

In our previous paper,[2,3] we analyzed concentration profiles by accounting for the linear terms in the expansion of the function $C^*_i = C^*_i(U)$ by powers of the substrate speed U. Accordingly, the validity of the results obtained in refs 2 and 3 is restricted to low magnitudes of both the velocities and concentration changes. It should be noted that appreciable changes in the adhesion work are expected for sufficiently big changes in the substrate composition.[8−10] Therefore, it is required to study the behavior of the function $C^*_i = C^*_i(U)$ within a wide range of the substrate velocities.

The objective of the present paper is to determine the functions $C^*_i(U)$ by considering the concentration polarization for a steady-state regime of withdrawing the substrate with a given velocity U. Having obtained the functions $C^*_i(U)$, we will analyze how the concentration polarization affects the behavior of the dynamic contact angle and dynamics of wetting. In particular, we will consider the role of concentration polarization in the meniscus instability, which is observed experimentally.

2. Description of the System

Let us consider the sketch illustrating the case of the Y-type LB deposition of the fatty acid (RH) monolayer onto a solid substrate (Figure 1). During such a process, the substrate is covered by a monolayer of the same molecules and is withdrawn upward with the speed U. Assuming that the transfer ratio is unity, the monolayer at the gas−liquid interface is transferred with the speed U as well.

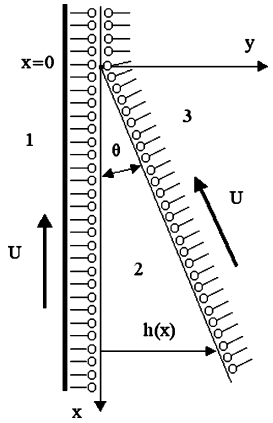

Figure 1. Sketch of LB film deposition process: (1) substrate, (2) liquid subphase, and (3) air.

Both monolayers are assumed to be in contact with a liquid subphase containing hydrogen ions (H^+), cations of a bivalent metal (M^{2+}), and anions (A^-). An aqueous solution of HCl and $CdCl_2$ is an example of such a subphase. The ion exchange between the monolayer and the subphase is provided due to the following reactions:

$$R^- + H^+ \leftrightarrow RH \tag{3}$$

$$2R^- + M^{2+} \leftrightarrow R_2M \tag{4}$$

$$R^- + M^{2+} \leftrightarrow RM^+ \tag{5}$$

where $R^- = CH_3(CH_2)_nCOO^-$ are the fatty acid anions and R_2M and RM^+ are two types of complexes formed by the fatty acid with the bivalent metal ions.

At the monolayers, due to the reactions described by eqs 3−5, there are complexes bearing positive (RM^+), negative (R^-), and zero charges (R_2M and RH). Notations for the interfacial concentrations of the complexes, X_k, are given in Table 1. The charged complexes form the interfacial charge, whose density is given by

$$\sigma = -F(X_{R^-} - X_{RM^+}) \tag{6}$$

Assuming that the interfacial equilibrium is established infinitely fast, all the interfacial concentrations, X_k, are functions of the concentrations of the hydrogen and metal ions in the immediate vicinity of each interfaces, $C^S_{H^+}$ and $C^S_{M^{2+}}$. Explicit forms of such functions, $X_k(C^S_{H^+},C^S_{M^{2+}})$, are determined from the equation set containing the equilibrium conditions for the reactions given by eqs 3−5

$$X_{RH} = K_H X_{R^-} C^S_{H^+} \tag{7}$$

$$X_{R_2M} = K_{M2}(X_{R^-})^2 C^S_{M^{2+}} \tag{8}$$

$$X_{RM^+} = K_{M1} X_{R^-} C^S_{M^{2+}} \tag{9}$$

and the conservation law for the fatty acid molecules being in all forms

$$X_R = X_{R^-} + X_{RH} + 2X_{R_2M} + X_{RM^+} \tag{10}$$

TABLE 1: Interfacial Concentrations of Complexes Formed by Fatty Acid with Different Ions

k	interfacial complex	charge	$X_k(C^S_{H^+},C^S_{M^{2+}})$
1	X_{RM^+}	1	$(1+K_HC^S_{H^+}+K_{M1}C^S_{M^{2+}})\frac{K_{M1}}{4K_{M2}}\left[\sqrt{1+\frac{8X_RK_{M2}C^S_{M^{2+}}}{(1+K_HC^S_{H^+}+K_{M1}C^S_{M^{2+}})^2}}-1\right]$
2	X_{RH}	0	$\frac{(1+K_HC^S_{H^+}+K_{M1}C^S_{M^{2+}})K_HC^S_{H^+}}{4K_{M2}C^S_{M^{2+}}}\left[\sqrt{1+\frac{8X_RK_{M2}C^S_{M^{2+}}}{(1+K_HC^S_{H^+}+K_{M1}C^S_{M^{2+}})^2}}-1\right]$
3	X_{R^-}	−1	$\frac{(1+K_HC^S_{H^+}+K_{M1}C^S_{M^{2+}})}{4K_{M2}C^S_{M^{2+}}}\left[\sqrt{1+\frac{8X_RK_{M2}C^S_{M^{2+}}}{(1+K_HC^S_{H^+}+K_{M1}C^S_{M^{2+}})^2}}-1\right]$
4	X_{R_2M}	0	$\frac{(1+K_HC^S_{H^+}+K_{M1}C^S_{M^{2+}})^2}{16K_{M2}C^S_{M^{2+}}}\left[\sqrt{1+\frac{8X_RK_{M2}C^S_{M^{2+}}}{(1+K_HC^S_{H^+}+K_{M1}C^S_{M^{2+}})^2}}-1\right]^2$

In eqs 7−10, K_H, K_{M1}, and K_{M2} are the equilibrium constants for the corresponding chemical reactions, and X_R is the total interfacial concentration of the fatty acid molecule. For given K_{M2}, K_{M1}, and X_R, one can solve equation set eqs 6−9 for obtaining the interfacial concentration of each complex as a function of $C^S_{H^+}$ and $C^S_{M^{2+}}$, $X_k(C^S_{H^+},C^S_{M^{2+}})$. The results of such calculations are collected in Table 1.

Taking the functions X_{R^-} $(C^S_{H^+},C^S_{M^{2+}})$ and X_{RM^+} $(C^S_{H^+},C^S_{M^{2+}})$ from Table 1, one can represent the interfacial charge density eq 6 as a function of the ionic concentration in the immediate vicinity of the interface, $\sigma(C^S_{H^+},C^S_{M^{2+}})$, as

$$\frac{\sigma}{F}=\frac{(1+K_HC^S_{H^+}+K_{M1}C^S_{M^{2+}})(1-K_{M1}C^S_{M^{2+}})}{4K_{M2}C^S_{M^{2+}}}\times\left[1-\sqrt{1+\frac{8X_RK_{M2}C^S_{M^{2+}}}{(1+K_HC^S_{H^+}+K_{M1}C^S_{M^{2+}})^2}}\right] \quad (11)$$

For all the complex situations to be considered next, we will assume that interfacial equlibrium holds. Consequently, during further ananalysis, we will use the functions $X_k(C^S_{H^+},C^S_{M^{2+}})$ (Table 1) and $\sigma(C^S_{H^+},C^S_{M^{2+}})$, eq 11.

3. Thermodynamic Equilibrium State

In the equlibrium state, all concentrations are distributed according to the Boltzmann law

$$C_{i(eq)}=C_i^\infty \exp[-z_iF\varphi_{eq}/RT] \quad (12a)$$

or, for concentrations in immediate vicinity of the interface, C_i^S

$$C^S_{i(eq)}=C_i^\infty \exp[-z_iF\varphi^S_{eq}/RT] \quad (12b)$$

where C_i^∞ and z_i are the bulk concentration and charge (in Faraday units) of the ith ions, respectively (see Table 2), R and F are the gas and Faraday constants, respectively, and T is the absolute temperature. Hence, by combining eq 11 with the expressions given in Table 1 and with eq 12b, both the interfacial group concentrations and charge density are represented as functions of the interfacial equilibrium potential φ^S_{eq} and ionic concentrations in the subphase bulk, $X_k(\varphi^S_{eq},C_i^\infty)$ and $\sigma(\varphi^S_{eq},C_i^\infty)$, respectively.

The distribution of the equilibrium electric potential φ_{eq} is determined as a solution of the Poisson Boltzmann equation

$$\nabla^2\varphi_{eq}=-\frac{F}{\epsilon_0\epsilon}\sum z_iC_i^\infty \exp[-z_iF\varphi_{eq}/RT] \quad (13)$$

TABLE 2: Ion Charges and Functions $B_i(C^{qe}_m)$

i	ion	z_i	B_i
1	H^+	1	$\frac{C^{qe}_{H^+}}{2(C^{qe}_{H^+}+3C^{qe}_{M^{2+}})}$
2	M^{2+}	2	$\frac{C^{qe}_{M^{2+}}}{(C^{qe}_{H^+}+3C^{qe}_{M^{2+}})}$
3	A^-	−1	$-\frac{C^{qe}_{H^+}+2C^{qe}_{M^{2+}}}{2(C^{qe}_{H^+}+3C^{qe}_{M^{2+}})}$

Subject to the boundary conditions

$$-\epsilon_0\epsilon\nabla\vec{\varphi}_{eq}\cdot\vec{n}=\sigma(\varphi^S_{eq},C_i^\infty) \quad \text{at the interfaces} \quad (14)$$

$$\varphi_{eq}\rightarrow 0 \quad \text{at infinity} \quad (15)$$

In eqs 13 and 14, ϵ is the dielectric permittivity of the subphase; $\vec{n}$ signifies the unit outward vectors normal to the interfaces.

We consider now the case that the gas−liquid interface has a small slope to the substrate. Then the above-presented problem can be simplified by using the Derjaguin approximation. Consequently, introducing the Cartesian coordinates x and y, as shown in Figure 1, and assuming that $\partial^2\varphi_{eq}/\partial x^2 \ll \partial^2\varphi_{eq}/\partial y^2$, eq 13 is rewritten as

$$\frac{\partial^2\varphi_{eq}}{\partial y^2}=-\frac{F}{\epsilon_0\epsilon}\sum z_iC_i^\infty \exp[-z_iF\varphi_{eq}/RT] \quad (16)$$

Boundary condition eq 14 is transformed as

$$\epsilon_0\epsilon\frac{\partial\varphi_{eq}}{\partial y}(0)=-\sigma(\varphi_{eq},C_i^\infty)$$

$$\epsilon_0\epsilon\frac{\partial\varphi_{eq}}{\partial y}[h(x)]=\sigma(\varphi_{eq},C_i^\infty) \quad (17)$$

where the function $y=h(x)$ describes the shape of the gas−liquid interface ($dh/dx \ll 1$).

Solution of the problem given by eqs 16 and 17 is the function $\varphi_{eq}(x, y, C_i^\infty) = \varphi_{eq}[h(x), y, C_i^\infty]$, which is represented by reversing the integrals

$$\begin{cases} y = -\mathrm{sign}(\varphi_{eq}^{S})\dfrac{\sqrt{\epsilon_0\epsilon RT/2}}{F}\displaystyle\int_{\varphi_{eq}^{S}}^{\varphi_{eq}} \frac{d\tilde{\varphi}}{\sqrt{\sum_i C_i^{\infty}[\exp(-z_i\tilde{\varphi}) - \exp(-z_i\tilde{\varphi}_{eq}^{m})]}} & \text{when } y < h(x)/2 \\ h(x) - y = -\mathrm{sign}(\varphi_{eq}^{S})\dfrac{\sqrt{\epsilon_0\epsilon RT/2}}{F}\displaystyle\int_{\varphi_{eq}^{S}}^{\varphi_{eq}} \frac{d\tilde{\varphi}}{\sqrt{\sum_i C_i^{\infty}[\exp(-z_i\tilde{\varphi}) - \exp(-z_i\tilde{\varphi}_{eq}^{m})]}} & \text{when } y > h(x)/2 \end{cases} \quad (18)$$

where $\tilde{\varphi}_{eq} = \varphi_{eq}F/RT$; the integration constant $\tilde{\varphi}_{eq}^{m}$ is determined as a solution of the equation set written with respect to two unknowns, $\tilde{\varphi}_{eq}^{m}$ and $\tilde{\varphi}_{eq}^{S}$

$$\sigma(\tilde{\varphi}_{eq}^{S}, C_i^{(0)}) = -\mathrm{sign}(\varphi_{eq}^{S})\frac{F}{\sqrt{\epsilon_0\epsilon RT/2}} \times \sqrt{\sum_i C_i^{\infty}[\exp(-z_i\tilde{\varphi}_{eq}^{S}) - \exp(-z_i\tilde{\varphi}_{eq}^{m})]} \quad (19)$$

$$h/2 = \mathrm{sign}(\varphi_{eq}^{S})\frac{\sqrt{\epsilon_0\epsilon RT/2}}{F}\int_{\varphi_{eq}^{m}}^{\varphi_{eq}^{S}} \times \frac{d\tilde{\varphi}}{\sqrt{\sum_i C_i^{\infty}[\exp(-z_i\tilde{\varphi}) - \exp(-z_i\tilde{\varphi}_{eq}^{m})]}} \quad (20)$$

Thus, for a given meniscus profile, $h(x)$, eqs 18−20 describe the equilibrium potential distribution, $\varphi_{eq}(x,y,C_i^{\infty})$, which is also a function of the subphase composition (the set of the bulk concentrations C_i^{∞}). The obtained interfacial potential is a function of x or h, as

$$\varphi_{eq}^{S}[x(h)] = \varphi_{eq}(x,0,C_i^{\infty}) = \varphi_{eq}(x(h),0,C_i^{\infty}) = \varphi_{eq}(x(h),h,C_i^{\infty}) \quad (21)$$

where $x(h)$ is obtained by reversing the function $h(x)$. The concentrations of ions in close vicinity to the interfaces are given by

$$C_{H^+(eq)}^{S}(h,C_i^{\infty}) = C_{H^+}^{\infty}\exp[-F\varphi_{eq}^{S}(h,C_i^{\infty})/RT]$$
$$C_{M^{2+}(eq)}^{S}(h,C_i^{\infty}) = C_{M^{2+}}^{\infty}\exp[-2F\varphi_{eq}^{S}(h,C_i^{\infty})/RT] \quad (22)$$

Combining eq 22 with the results given in the last column of Table 1, the concentration of the interfacial group can be represented as functions of subphase bulk composition and h (or x), $X_k(h,C_i^{\infty})$. Similarly, combining eqs 11 and 22, one obtains the function $\sigma(h,C_i^{\infty})$. For more details regarding the equilibrium state of the system, see ref 13.

4. Dynamic Regime

Now, using the Cartesian coordinates shown in (Figure 1), we consider the steady-state distribution of ions when the substrate moves with the upward speed U. Approximating the interface by a plane and assuming that the contact angle, θ, is small, one obtains

$$h(x) \approx \theta \cdot x \quad (23)$$

The analysis is conducted using the lubrication approximation. Consequently, we assume that the pressure and the electrochemical potential of ions, μ_i^{el}, do not depend on y. As well, we ignore the changes in the velocity distribution that are produced due to changes of concentrations and electric potential.

According to de Gennes,[7] within the framework of the lubrication approximation for sufficiently small θ, the subphase flow around the three-phase contact line can be described as

$$\vec{u}(x,y) = U\left[-\frac{1}{2} + 6\left(\frac{y}{h(x)} - \frac{1}{2}\right)^2\right]\vec{\imath}_x \quad (24)$$

At deriving eq 24, the volume of the solution component withdrawn with the film is assumed to be negligible.

4.1. Balance and Electrostatic Equations. In the steady-state regime, the flux of the ith ion through any of the cross-sections is a constant value that is equal to the number of the ith ions being removed by the deposited film per unit of time. Because each of the fluxes consists of an interfacial (J_i^S), convective (J_i^C), and electro-diffusion (J_i^{ED}) components, the steady-state mass balance equation for the ith ion takes the form[2,3]

$$J_i^S + J_i^C + J_i^{ED} = 2U\sum_k \nu_{ik}X_k^{Dep} \quad (25)$$

where

$$J_i^S = 2U\sum_k \nu_{ik}X_k \quad (26)$$

$$J_i^C = \int_0^{h(x)} u(y,x)C_i(x,y)dy \quad (27)$$

$$J_i^{ED} = -D_i\int_0^{h(x)} \frac{C_i(x,y)}{RT}\frac{\partial\mu_i^{el}}{\partial x}dy \quad (28)$$

In eqs 25−28, $u(x,y)$ is given by eq 24, D_i is the ith ion diffusion coefficient, X_k^{Dep} and X_k, respectively, are the interfacial concentrations of the kth chemical complex existing in the deposited film and at the interfaces, and ν_{ik} is the number of the ith ions inside the kth complex. For the system under consideration, using the numeration of the interfacial groups and ions given in Tables 1 and 2, the matrix $||\nu||$ takes the form

$$||\nu|| = \begin{pmatrix} 0 & 1 & 0 & 0 \\ 1/2 & 0 & 0 & 1 \\ 0 & 0 & 0 & 0 \end{pmatrix} \quad (29)$$

Considering an ideal electrolyte solution, the differential of the electrochemical potential μ_i^{el} is given by

$$d\mu_i^{el} = z_iFd\varphi + RTd(\ln C_i) \quad (30)$$

where φ is the local electric potential satisfying the Poisson equation, which, using the Derjaguin approximation, can be written as

$$\frac{\partial^2\varphi}{\partial y^2} = -\frac{F}{\epsilon_0\epsilon}\sum_i C_i z_i \tag{31}$$

Equation 31 is subject to the Derjaguin approximation version of boundary condition

$$\epsilon_0\epsilon\frac{\partial\varphi}{\partial y}(0) = -\sigma(C_i^S)$$

$$\epsilon_0\epsilon\frac{\partial\varphi}{\partial y}[h(x)] = \sigma(C_i^S) \quad \text{at the interfaces} \tag{32}$$

$$\varphi_{eq} \rightarrow 0 \quad \text{at infinity} \tag{33}$$

Within the framework of the lubrication approximation, μ_i^{el} is assumed to be independent of y. Therefore, one can take $\partial\mu_i^{el}/\partial x$ out of the integral in eq 28. Consequently, combining eqs 24−30 one obtains

$$\frac{d\mu_i^{el}}{dx}\frac{D_i}{RT}\int_0^{h(x)} C_i(x,y)dy = -U\left[2\sum_k \nu_{ik}(X_k^{Dep} - X_k) - \int_0^{h(x)}\left(-\frac{1}{2} + 6\left(\frac{y}{h} - \frac{1}{2}\right)^2\right)C_i(x,y)dy\right] \tag{34}$$

The following steps in reducing the equations are associated with a substitution, which is considered next.

4.2. Variable Substitution and Reduction of the Problem. Let us introduce a new set of unknown variables, C_i^{qe}, Ψ, and Φ, according to the following substitution[5]

$$C_i(x,y) = C_i^{qe}(x,y)\exp[-z_i F\Psi(x,y)/RT] \tag{35}$$

$$\varphi(x,y) = \Psi(x,y) + \Phi(x,y) \tag{36}$$

Note that instead of $N+1$ unknowns (N = number of ions), C_i and φ, we introduced $N+2$ unknowns, C_i^{qe}, Ψ, and Φ. To interrelate the new and old variables in a unique manner, we will introduce an additional condition

$$\sum_i z_i C_i^{qe}(x,y) = 0 \tag{37}$$

From a purely mathematical point of view, eqs 35−37 can be considered as a formal substitution of variables. At the same time, the new variables C_i^{qe}, Ψ, and Φ have a clear physical meaning that can be understood while considering an electroneutral electrolyte solution being in thermodynamic equilibrium with a given point of the analyzed system.[5] To such a solution, which may not be presented in a real physical system (but can be always found), we refer to a virtual solution. Consequently, C_i^{qe} is the ith ion concentration in the virtual solution and Ψ is the electric potential difference that would occur between a given point of the system under consideration and the virtual solution. A difference in the potentials, Φ, is a difference between electric potentials attributed to different virtual solutions that are equilibrated with different points of the real system.

While considering infinitely slow deposition, the system shown in Figure 1 is in an actual thermodynamic equilibrium state. For the latter case, the bulk electrolyte solution, where the ionic concentrations is C_i^{∞}, coincides with the virtual solution. Consequently, for infinitely slow deposition, Ψ coincides with the equilibrium potential, φ_{eq}, given by a solution of the Poisson−Boltzmann problem.[1,2] As for the variables Φ and C_i^{qe}, they do not depend on the coordinates in the equilibrium state because $\Phi = 0$ and $C_i^{qe} = C_i^{\infty}$.

When the deposition rate is sufficiently high, C_i^{qe} and Φ become space dependent. To analyze these dependencies, we substitute eqs 35 and 36 in eq 30

$$d\mu_i^{el} = z_i F d\Phi + RT d(\ln C_i^{qe}) \tag{38}$$

Recalling the assumption that μ_i^{el} is independent of y (lubrication approximation), eq 38 leads to the conclusion that both C_i^{qe} and Φ are independent of y as well. Thus, using the lubrication approximation, eqs 35 and 36 can be simplified as

$$C_i(x,y) = C_i^{qe}(x)\exp[-z_i F\Psi(x,y)/RT] \tag{39}$$

$$\varphi(x,y) = \Psi(x,y) + \Phi(x) \tag{40}$$

Combining eqs 31−33, 39, and 40 we arrive at the following equation for obtaining $\Psi(x,y)$

$$\frac{\partial^2\Psi}{\partial y^2} = -\frac{F}{\epsilon_0\epsilon}\sum_i z_i C_i^{qe}(x)\exp(-z_i F\Psi/RT) \tag{41}$$

$$\epsilon_0\epsilon\frac{\partial\Psi}{\partial y}(0) = -\sigma[\Psi^S, C_i^{qe}(x)]$$

$$\epsilon_0\epsilon\frac{\partial\Psi}{\partial y}[h(x)] = \sigma[\Psi^S, C_i^{qe}(x)] \tag{42}$$

Comparing eqs 41−42 with eqs 16−17, we arrive at the conclusion that $\Psi(x,y)$ can be directly obtained from the already known equilibrium potential distribution, $\varphi_{eq}[h(x),y,C_i^{\infty}]$ (see eqs 18−20). It is only necessary to replace in $\varphi_{eq}[h(x),y,C_i^{\infty}]$ the space-independent bulk concentration of ions, C_i^{∞}, by their quasi-equilibrium concentrations, $C_i^{qe}(x)$, being functions of x.

$$\Psi(x,y) = \varphi_{eq}[h(x),y,C_i^{qe}(x)] \tag{43}$$

Combining eq 34 and eq 43, we represent each of the electrochemical potential gradients, $\partial\mu_i^{el}/\partial x$ as a function of h and all the quasi-equilibrium concentrations. Consequently, using eq 23 one obtains

$$\frac{d\mu_i^{el}}{dh} = (-U/\theta)f_i[h, C_m^{qe}]$$

$$= \frac{(-U/\theta)\left\{\frac{2}{C_i^{qe}}\sum_k \nu_{ik}[X_k^{Dep}(0, C_m^{qe*}) - X_k(h, C_m^{qe})] - \beta_i(h, C_m^{qe})\right\}}{\frac{D_i}{RT}\alpha_i(h, C_m^{qe})} \tag{44}$$

where C_m^{qe*} is the mth ion quasi-equilibrium concentration in the immediate vicinity of the three-phase contact line

$$\alpha_i(h, C_m^{qe}) = \int_0^h \exp[-z_i\tilde{\varphi}_{eq}(h,y,C_m^{qe})]dy \tag{45}$$

$$\beta_i(h, C_m^{qe}) = \int_0^h\left(-\frac{1}{2} + 6\left(\frac{y}{h} - \frac{1}{2}\right)^2\right)\exp[-z_i\tilde{\varphi}_{eq}(h,y,C_m^{qe})]dy \tag{46}$$

In eq 44, the functions $X_k(h,C_m^{eq})$ are determined using the expressions given in the last column of Table 1. In these expressions, instead of the concentrations C_i^S ($C_{H^+}^S$ and $C_{M^{2+}}^S$), one should substitute $C_i^{qe} \exp[-z_i\tilde{\varphi}_{eq}^S(h,C_m^{qe})]$.

Combining eqs 37, 38, and 44, one obtains a set of ordinary differential equations with respect to the unknown functions $C_i^{qe}(h)$.

$$\frac{d}{dh}\ln(C_i^{qe}) = \frac{(-U/\theta)}{RT}\sum_m [\delta_{mi} - z_i B_m(C_n^{qe})] f_m(h,C_n^{qe}) \quad (47)$$

where δ_{mi} − are the Kronecker's deltas and

$$B_m(C_n^{qe}) = \frac{C_m^{qe} z_m}{\sum_l C_l^{qe} z_l^2} \quad (48)$$

For the ions presented in the system under consideration, explicit expressions for $B_m(C_n^{qe})$ are given in Table 2.

It should be noted that, by definition, the quasi-equilibrium concentrations satisfy eq 37, which was employed to derive eq 47. Therefore, for N ions, equation set eq 47 gives $N-1$ independent equations intended for obtaining $N-1$ quasi-equilibrium concentrations. Accordingly, the Nth concentration is determined using eq 37.

To obtain a closed problem formulation, equation set eq 47 should be subject to a set of boundary conditions. Such a necessity originates from the assumption regarding the planar geometry of the air−water interface. For such a geometry, considering the variation of the coordinate x within the range $0 < h < \infty$, it is impossible to obtain a steady-state problem solution. However, a correct solution, which is close to the steady state, can be obtained for the case if an actual nonplanar shape of the meniscus is taken into account. For the latter situation, one should set the boundary conditions at infinity by equating the quasi-equilibrium and bulk concentrations (C_i^{qe} and C_i^{∞}).

For the above-mentioned "correct" concentration distributions, the major concentration changes are expected to be localized within the range $0 < h < l$, where l is the length scale parameter describing the meniscus shape (capillary length, for example). Accordingly, to approach the "correct" distributions, we will set the following boundary conditions

$$C_i^{qe}(l) = C_i^{\infty} \quad (49)$$

Thus, the solution of the equation set given by eq 47 subject to the boundary conditions given by eq 49 yields $N-1$ quasi-equilibrium concentrations, C_i^{qe}, (for example, $C_{H^+}^{qe}$ and $C_{M^{2+}}^{qe}$). Then, using eq 37, one obtains the Nth concentration ($C_{A^-}^{qe}$). The concentrations are obtained in the form

$$C_i^{qe} = C_i^{qe}(U/\theta,h,C_m^{qe^*}) \quad (50)$$

Due to the structure of the functions $f_m(h,C_n^{qe})$ that are represented in eq 47 and defined by eq 44, each of the concentrations depends on a set of unknown quantities, $C_m^{qe^*}$, having the meaning of the quasi-equilibrium concentrations in immediate vicinity to the three-phase contact line. These quantities are determined from the equation set that follows from eq 50

$$C_i^{qe^*} = C_i^{qe}(U/\theta,0,C_m^{qe^*}) \quad (51)$$

After obtaining the concentration set C_i^{qe}, one can determine the distribution of the newly introduced unknown function $\Phi(h)$. Combining eqs 37, 38, and 44 yields

$$\frac{d}{dh}\Phi = \frac{(-U/\theta)}{F}\sum_m B_m f_m(h,C_n^{qe}) \quad (52)$$

Thus, the above-formulated problem enables one to find the unknown functions $\Psi[y,C_i^{qe}(U/\theta,x)]$, $C_i^{qe}[U/\theta,h(x)]$, and $\Phi[U/\theta,h(x)]$. In principle, using eqs 39 and 40, one can reconstruct the original (actual) concentrations and potential, C_i and φ. Sometimes, such a reconstruction is not necessary because the newly introduced functions bear the required information in a more convenient form.

Using the quasi-equilibrium rather than actual concentrations, it is more convenient to analyze the influence of the concentration polarization on the adhesion work, which, consequently, affects the contact angle and the unbalanced force. Assuming the interfacial quasi-equilibrium for the dynamic regime, the adhesion work is defined by the quasi-equilibrium concentrations in the immediate vicinity of the three-phase contact line, $C_i^{qe^*}$. Remarkably, such a value of the adhesion work is equal to that attributed to a thermodynamic equilibrium state, provided that the bulk electrolyte concentrations C_i^{∞} coincide with $C_i^{qe^*}$.

5. Results

For any ionic composition of the subphase, the above-formulated approach can be applied to address the deposition of monolayers of different types. In the present work, we will analyze the results for a particular case of a fatty acid (e.g., stearic, arachidic, behenic acids) monolayer in contact with a subphase containing a cadmium salt (e.g. $CdCl_2$) and an inorganic acid (e.g. HCl). The features of such a system is in the focus of many experimental studies beginning from the classical works of Langmuir and Blodgett.[14,15]

To address the behavior of the above-mentioned system, the problem, given by eqs 37, 47, and 52 and subject to the boundary condition eq 49, was numerically solved within the region described by the inequality $0 < h(x) < l$. The reference point for the potential was chosen at $h = l$, i.e., $\Phi(l) = 0$. Using Table 2, the functions $f_m(h,C_n^{qe})$ and $B_m(C_n^{qe})$ represented in eqs 47 and 52 are obtained from eq 48. To conduct each of the subsequent integration steps, it is necessary to know the quasi-equilibrium potential distribution $\Psi(x,y)$, which is a solution of the problem given by eqs 41−42.

The cadmium and hydrogen ion concentrations within the subphase, $C_{Cd^{2+}}^{\infty}$ and $C_{H^+}^{\infty}$, were varied within a wide range. The values of the ion diffusion coefficients were chosen as $D_{H^+} = 9.34 \times 10^{-9}$ m^2/s, $D_{Cd^{2+}} = 7.2 \times 10^{-10}$ m^2/s, and $D_{Cl^-} = 2.04 \times 10^{-9}$ m^2/s. For the constants describing interfacial chemical equilibrium, we have chosen the same values as in our previous studies, i.e., $K_H = 6.54 \times 10^4$ dm^3/mol, $K_{M1} = 15.5$ dm^3/mol, and $K_{M2} = 2.5 \times 10^9$ dm^5/mol^2.[1−3,13] For stoichiometry of the interfacial fatty acid complexes, we considered all the models discussed in the literature: (i) neutral R_2M complexes, only;[16] (ii) positively charged RM^+ complexes, only;[17] and (iii) both above types of complexes, simultaneously.[18] According to our calculations, model ii yields nearly the same behavior as model iii. Therefore, the discussion given below is only concerned with models i and iii.

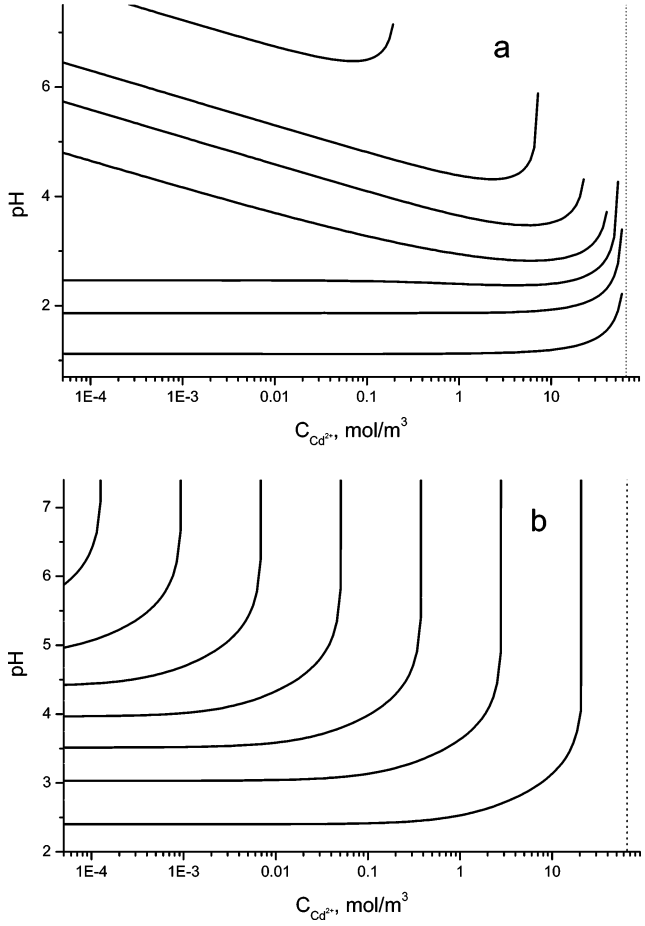

Figure 2. Diagrams $\sigma(C^{\infty}_{H^+},C^{\infty}_{M^{2+}})$ and $\varphi^{S}_{eq}(C^{\infty}_{H^+},C^{\infty}_{M^{2+}})$ for a fatty acid monolayer under equilibrium conditions (both R_2M and RM^+ complexes): (a) lines of constant surface charge density (in percents to FX_R,) correspond to 0.02%, 0.1%, 0.25%, 0.5%, 1.0%, 1.5%, and 1.75% from bottom to top; (b) lines of constant surface potential (normalized by F/RT) correspond to 0.5, 1.5, 2.5, 3.5, 4.5, 5.5, and 6.5 from bottom to top (the dotted lines at $C^{\infty}_{Cd^{2+}} = 65$ mol/m^3 correspond to zero charge).

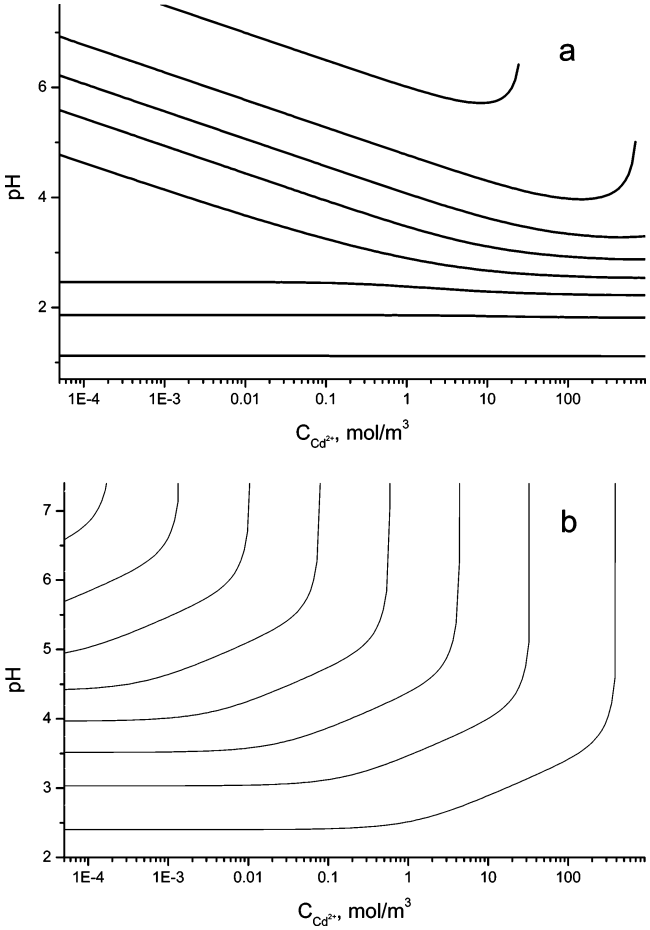

Figure 3. Diagrams $\sigma(C^{\infty}_{H^+},C^{\infty}_{M^{2+}})$ and $\varphi^{S}_{eq}(C^{\infty}_{H^+},C^{\infty}_{M^{2+}})$ for a fatty acid monolayer under equilibrium conditions (only R_2M complexes): (a) lines of constant surface charge (in percents to FX_R,) correspond to 0.02%, 0.1%, 0.25%, 0.5%, 1.0%, 2.0%, 4.0%, and 5.75% from bottom to top; (b) lines of constant surface potential (normalized by F/RT) correspond to 0.5, 1.5, 2.5, 3.5, 4.5, 5.5, 6.5, and 7.5 from bottom to top.

Usually, fatty acid monolayers are deposited at sufficiently high surface pressures (25−30 mN/m). Under such conditions, the monolayers are in a close-packed (condensed) state. Consequently, such parameters as the surface area per molecule and, hence, the total interfacial concentration of fatty acid (X_R) are nearly independent of both the surface pressure and the subphase composition.[19] Having assumed X_R to be constant, we set $X_R = 8.3 \times 10^{-6}$ mol/m^2, which is a quite typical value for the fatty acid monolayers.

5.1. Equilibrium State. The equilibrium state of monolayers in the meniscus region is described as discussed in sections 2 and 3. For an individual (out of the meniscus region) fatty acid monolayer being under equilibrium conditions, the diagrams in Figures 2 and 3 describe the behavior of surface charge density and potential as functions of the cadmium and hydrogen ion concentrations within the subphase ($\sigma(C^{\infty}_{H^+},C^{\infty}_{M^{2+}})$ and $\varphi^{S}_{eq}(C^{\infty}_{H^+}, C^{\infty}_{M^{2+}})$, respectively). The diagram in Figure 2 corresponds to the case that both types of the complexes, R_2M and RM^+, are present in the monolayer (model iii), whereas Figure 3 displays the case that only neutral R_2M complexes are formed (model i).

It is seen that, at small cadmium concentrations, both surface charge density and surface potential increase as pH increases. This dependence becomes very weak at high pH values and/or high cadmium ion concentrations. At high pH values, with decreasing cadmium concentration, the surface charge density initially increases and then decreases, passing through a maximum. At small cadmium concentrations ($C^{\infty}_{Cd^{2+}} < 10^{-3}$ M), the curves displaying the dependencies of surface charge density on pH have two transition regions. When pH is around 2, the surface charge density increases because of the dissociation of fatty acid molecules. At higher pH, the surface charge density increases again because of the monolayer conversion from the hydrogen form to the cadmium form. For pH < 7, the surface charge density does not exceed 2% (model iii) or 6% (model i) of the maximum possible charge density corresponding to a complete dissociation of the carboxylic groups at the interface (FX_R).

There is a remarkable difference in the properties of monolayers in the presence and in the absence of the positively charged complexes RM^+. According to eqs 6 and 9, in the presence of RM^+ complexes, the surface charge should become zero at the concentration of cadmium ions $C^{\infty}_{Cd^{2+}} = 1/K_{M1} = 0.065$ M. Moreover, at higher concentrations, a sign reversion is observed for the interfacial charge. In the absence of RM^+ complexes, the charge reversion does not occur. Nevertheless, for both models under usual conditions for the LB films deposition at the monolayer, the ratio of hydrogen to cadmium ions, $X_{RH}/(X_{R_2M} + X_{RM^+})$ remains nearly the same. Hence, the

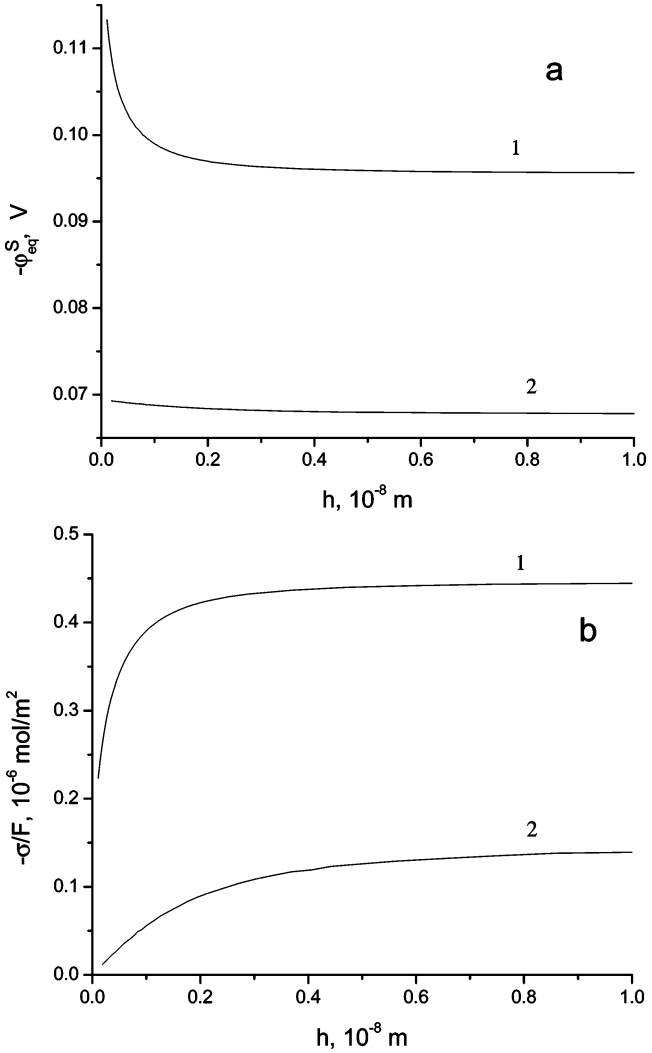

Figure 4. (a) Variation of the surface potential and (b) surface charge density (in Faraday units), with the distance between the charged surfaces in the case of (1) only R_2M complexes and (2) both R_2M and RM^+ complexes ($pH_\infty = 5.7$, $C^\infty_{Cd^{2+}} = 2.5 \times 10^{-4}$ M).

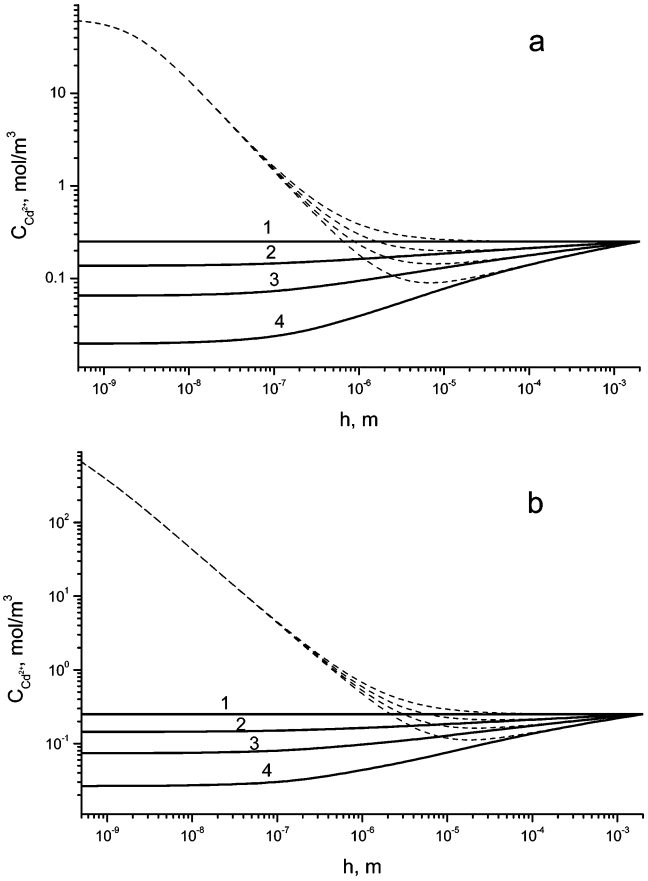

Figure 5. Profiles of quasi-equilibrium (full lines) and average (dashed lines) concentrations of cadmium ions in the meniscus region for different velocities: U/θ = (1) 0 cm/s, (2) 0.25 cm/s, (3) 0.5 cm/s, and (4) 0.8 cm/s ($pH_\infty = 5.7$, $C^\infty_{Cd^{2+}} = 2.5 \times 10^{-4}$ M, (a) both R_2M and RM^+ complexes and (b) only R_2M complexes).

experimental data about the deposited film composition do not yield information about which model of the interfacial group stoichiometry (i, ii, or iii) is preferable.

In the meniscus region, the diffuse layers formed at the liquid/solid and air/liquid interfaces are overlapping, provided that the distance between the interfaces is of the order of the Debye length. Due to the overlap of the diffuse layers within such a region, the equilibrium surface potential φ^S_{eq} increases and becomes a function of the local distance between the interfaces h (Figure 4a). Consequently, the local concentrations $C^S_{H^+}$ and $C^S_{M^{2+}}$ increase and the surface charge density decreases in this region. Thus, the surface charge density becomes also dependent on the distance h (Figure 4b) and approaches to zero at the three-phase contact line. When accounting for the neutral R_2M interfacial complexes only, the surface potential infinitely increases toward the three-phase contact line, whereas accounting for the RM^+ complexes, the increasing surface potential approaches to a limiting value $|\varphi^S_{lim}| = -(RT/2F)\ \ln(K_{M1} C^\infty_{Cd^{2+}})$, as follows from eq 6.

5.2. Dynamic Regime. In Figures 5−7, the concentrations and potential profiles in the meniscus region are shown for the case of dynamic conditions. As discussed above, these profiles develop for each sort of ions because of a misbalance between the number of ions removed from the solution by the deposited film and transported due to convection toward the three-phase contact line. The larger the deposition rate, the larger the misbalances and the sharper the profiles. Far from the contact line (for large distances h), the quasi-equilibrium concentrations, C^{qe}_i, change relatively slowly (Figures 5 and 6). The most significant changes of the quasi-equilibrium concentrations are observed in the regions with a weak overlap of the diffuse layers. The overall changes of quasi-equilibrium concentrations are mainly localized out of the regions of strong overlap.

For sufficiently large distances between the interfaces, being averaged over the meniscus cross-section, the actual concentrations of counterions nearly coincide with C^{qe}_i. At the distances where the diffuse layers begin to overlap, the average actual concentrations become larger than C^{qe}_i (Figures 5 and 6). Therefore, toward the contact line, the average concentrations initially decrease simultaneously with C^{qe}_i and then increase, showing a minimum in a transition region. In the region of small h within the subphase, the actual concentrations of counterions exceed the quasi-equilibrium concentrations by some orders of magnitude. The latter takes place because the counterions are accumulated for neutralizing the oppositely charged interfacial groups. Oppositely, the concentration of coions is strongly suppressed in this region.

The profiles of the potential Φ are shown in Figure 7. The difference in the potentials Φ between the close vicinity of the contact line and the regions in the bulk solution is clearly seen.

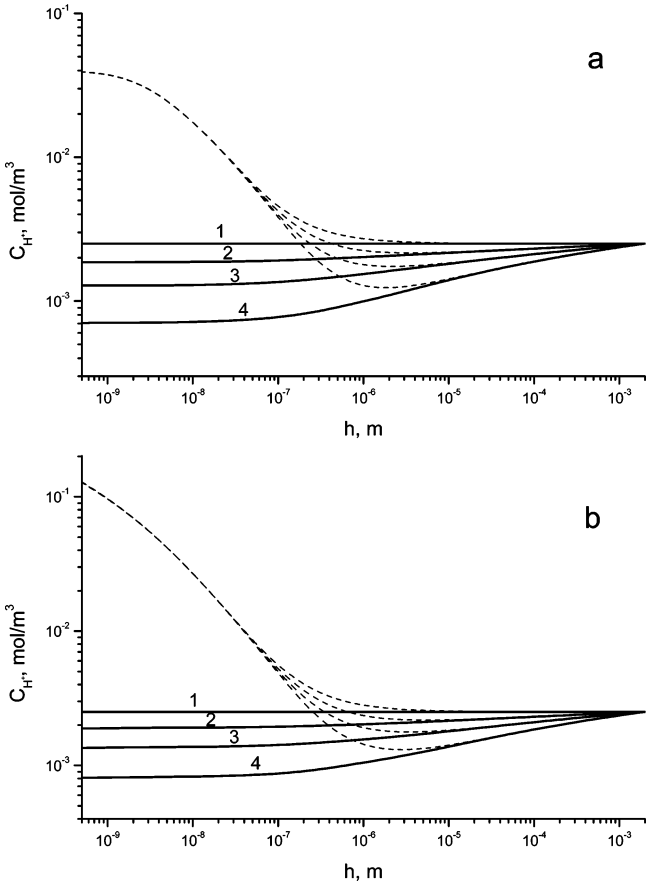

Figure 6. Profiles of quasi-equilibrium (full lines) and average (dashed lines) concentrations of hydrogen ions in the meniscus region for different velocities: U/θ = (1) 0 cm/s, (2) 0.25 cm/s, (3) 0.5 cm/s, and (4) 0.8 cm/s ($pH_\infty = 5.7$, $C^\infty_{Cd^{2+}} = 2.5 \times 10^{-4}$ M, (a) both R_2M and RM^+ complexes and (b) only R_2M complexes).

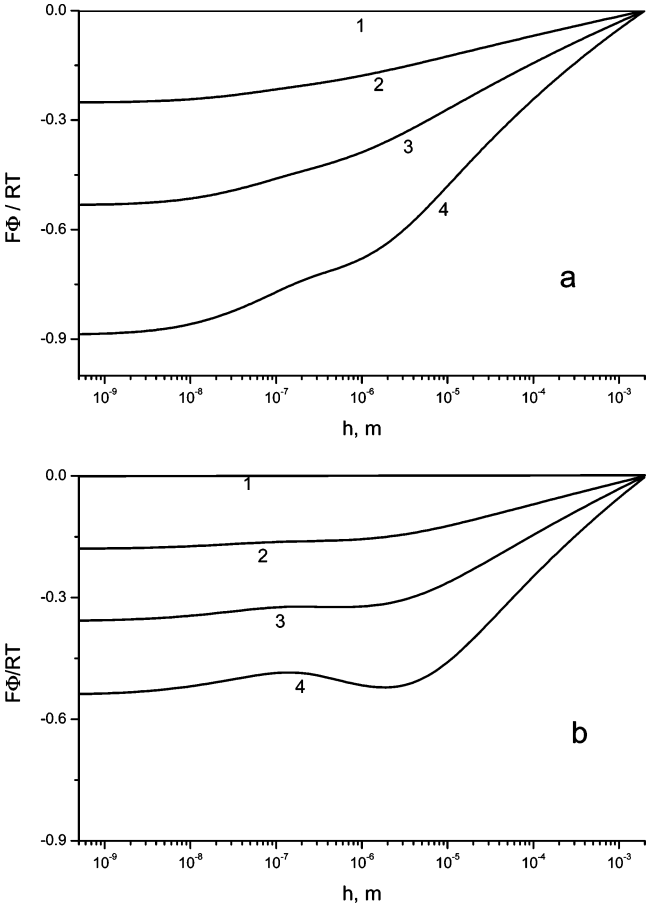

Figure 7. Profiles of the potential Φ in the meniscus region for different velocities: U/θ = (1) 0 cm/s, (2) 0.25 cm/s, (3) 0.5 cm/s, and (4) 0.8 cm/s ($pH_\infty = 5.7$, $C^\infty_{Cd^{2+}} = 2.5 \times 10^{-4}$ M, (a) both R_2M and RM^+ complexes and (b) only R_2M complexes).

According to eqs 25 and 37, the gradient of the potential, Φ, can be represented as a sum of two terms

$$\frac{\partial \Phi}{\partial h} = \frac{RT}{F\theta}\frac{\sum_i z_i(J_i^C + J_i^S)}{\sum_i z_i^2 C_i^{qe} D_i \alpha_i} - \frac{RT}{F}\frac{\sum_i z_i D_i \alpha_i \frac{\partial C_i^{qe}}{\partial h}}{\sum_i z_i^2 C_i^{qe} D_i \alpha_i} \quad (53)$$

where the first term describes the streaming potential and the second term yields the concentration potential. Note that in the first term, the sum in the numerator includes the flux of the charged interfacial groups. For different ions, the fluxes J_i^S and J_i^C and the concentration gradients change with the distance differently. Both parts in eq 53 include the contributions of negatively and positively charged ions. Therefore, the potential Φ changes with h non-monotonically (it is more clearly seen on curves 4 in Figure 7 plotted for the highest velocity U).

The potential and concentration profiles define the profiles of the electrochemical potentials of ions (eq 38) and, hence, the electro-diffusion components of the ion fluxes induced in the meniscus region. The behavior of the partial ion fluxes are shown in Figure 8. The flux $J_i^X = 2U\sum_k \nu_{ik}(X_k^{Dep} - X_k)$ is the total flux of the ith ion that is required to form complexes with fatty acid anions in the course of their transfer to the substrate surface. Under steady-state conditions, this flux should be equivalent to the sum of the convective and electro-diffusion fluxes determined for each meniscus cross-section. In the region where the diffuse layers overlap, the convective component of the ith ion flux decreases much more rapidly toward the contact line than the flux J_i^X. Therefore, in this region, the contribution of the electro-diffusion component increases.

At large distances between the interfaces, the convective component is large, and, therefore, the electro-diffusion component is small. Nevertheless, the electro-diffusion flux does not disappear, even at large distances (Figure 8). The latter is explained by a decrease in the coion concentration within the diffuse layers with respect to their bulk concentration. Due to this fact, the convective flux of coions is not zero at any distance. Accordingly, in the case of a steady-state regime, an equivalent (but oppositely directed) electro-diffusion flux of coions is necessary. As well, for complete neutralization of the monolayer charge, the purely convective flux of counterions is not sufficient at any distance, and thus, an additional electro-diffusion flux is required.

5.3. Immediate Vicinity of the Contact Line. It is seen from Figures 5 and 6 that in the region close to the three-phase contact line ($h < 10^{-8}$ m), the change of the quasi-equilibrium concentrations is very small as compared to their overall change. The overall change of the quasi-equilibrium concentrations increases with the velocity U. For sufficiently high velocities, the local concentrations in the immediate vicinity of the contact line can be much smaller than in the bulk solution. Figure 9 displays the dependencies of the quasi-equilibrium concentrations in this region, $C^{qe^*}_{Cd^{2+}}$ and $C^{qe^*}_{H^+}$, on the velocity U. It is seen

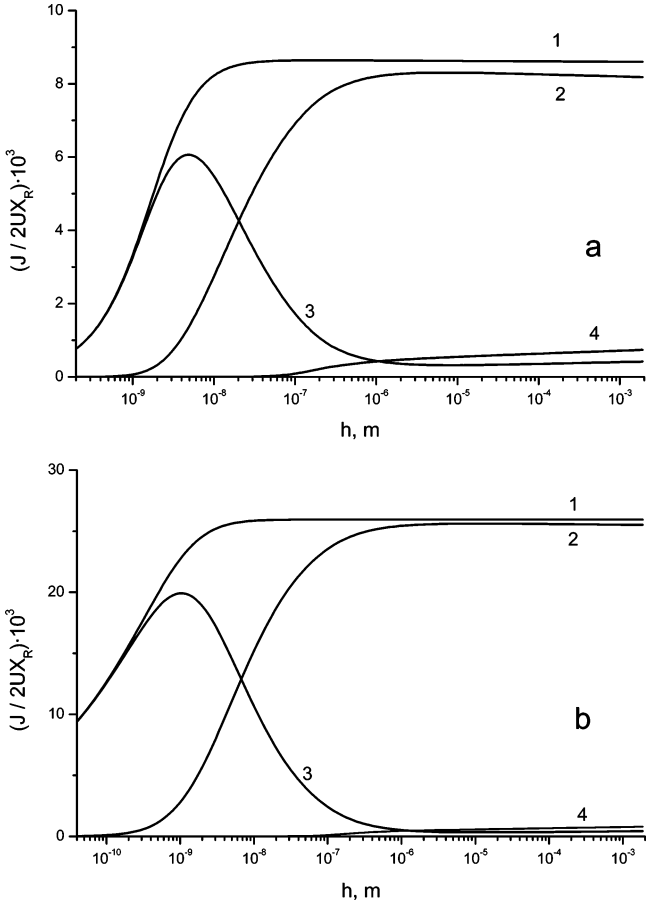

Figure 8. Partial ion fluxes of cadmium ions and coions (normalized by $2UX_R$) vs. distance between the interfaces for $U/\theta = 0.5$ cm/s: (1) total flux ($J^X_{Cd^{2+}}$), (2) convective flux ($J^C_{Cd^{2+}}$), and (3) electro-diffusion flux ($J^{ED}_{Cd^{2+}}$) of cadmium ions; (4) electro-diffusion flux of coions ($J^{ED}_{Cl^-} = -J^C_{Cl^-}$) ($pH_\infty = 5.7$, $C^\infty_{Cd^{2+}} = 2.5 \times 10^{-4}$ M, (a) both R_2M and RM^+ complexes and (b) only R_2M complexes).

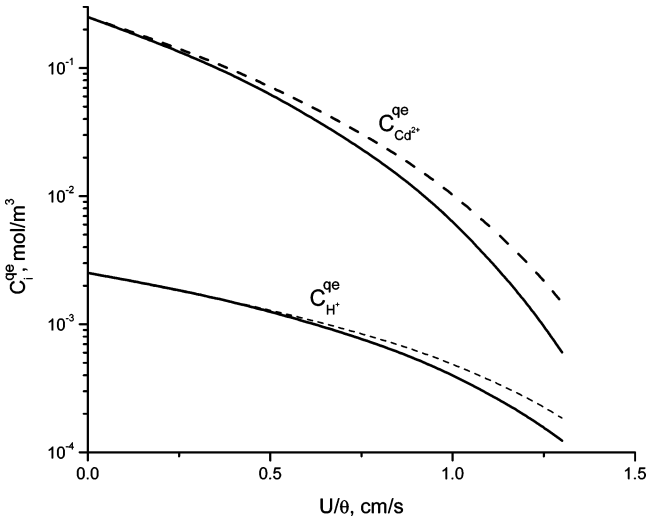

Figure 9. Dependencies of quasi-equilibrium concentrations of ions in the immediate vicinity of the three-phase contact line on the velocity U ($pH_\infty = 5.7$, $C^\infty_{Cd^{2+}} = 2.5 \times 10^{-4}$ M, both R_2M and RM^+ complexes (full lines) and only R_2M complexes (dashed lines)).

that, with increasing velocity, the decrease of the concentrations becomes more rapid, and the concentrations approach very small values.

The composition of the solution close to the contact line is defined by both the composition of bulk solution and the deposition rate. The latter is illustrated, in particular, by the diagram presented in Figure 10, where each of the curves is plotted for bulk solution compositions that correspond to the given values of the velocity, U, and the ionic strength, 10^{-7} mol/dm^3, evaluated using the quasi-equilibrium concentrations attributed to the contact line region. At a given ionic strength at the contact line, a higher velocity corresponds with higher bulk concentrations, $C^\infty_{Cd^{2+}}$ and $C^\infty_{H^+}$.

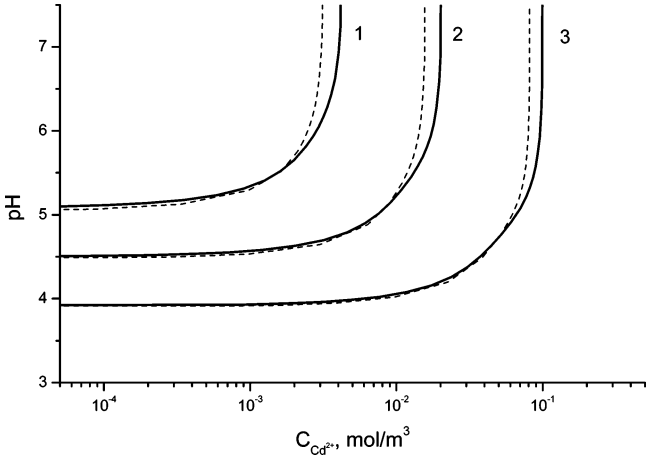

Figure 10. Diagram of compositions of bulk solution providing the constant ionic strength of 10^{-7} mol/dm^3 in the equilibrium (virtual) solution, related to the contact line region, for different velocities: U/θ = (1) 0.25 cm/s, (2) 0.5 cm/s, and (3) 1.0 cm/s (both R_2M and RM^+ complexes (full lines) and only R_2M complexes (dashed lines)).

6. Discussion

The results above-presented demonstrate clearly significant changes of the subphase composition in the immediate vicinity of the contact line. Such changes should be observed after a certain transition time after starting the substrate withdrawal. Such a transition time is required to reach a steady- (or quasi-steady-) state regime. Accordingly, after stopping the substrate motion, one can expect a slow relaxation process of ion redistribution while the system approaches to the equilibrium state. Such a slow relaxation dynamics has been observed in many experiments [9,10,20] after stopping the substrate motion.

To conclude whether the above-mentioned relaxation behavior can be explained through the slow redistribution of ions within a macroscopically large meniscus region, we will conduct the following evaluation. For the distances of about 1 mm and the ion diffusion coefficient of order of 10^{-9} m^2/s, the relaxation time for the concentration redistribution is about 10^3 s. The latter value is of the same order as that observed in experiments. For comparison, the hydrodynamic relaxation time $\tau_h = l^2/\nu$ (where ν = the kinematic viscosity, for water about 10^{-6} m^2/s) is much smaller—on the order of 1 s.

Although for finite deposition rates the equilibrium is absent as a whole in the system, the local equilibrium (quasi-equilibrium) conditions can hold within microscopically small regions. If, in the immediate vicinity of the contact line, the deviations from local equilibrium are small, then the ion concentrations in this region should define the interaction of the monolayer with the substrate surface as well as the composition and structure of the deposited film. Hence, the change of the local concentrations with the velocity U should affect the adhesion work and the shape of the air/water interface close to the contact line. The simplest change of the shape of the interface reveals itself as a change of the contact angle.

When the dependencies $W = W(C^*_{i(eq)})$ and/or $\theta = \theta_e(C^*_{i(eq)})$ are known, for example, from experimental data obtained under equilibrium conditions, then the effect of the deposition rate on these characteristics can be understood by accounting for the obtained above dependencies $C_i^{qe*}(U)$. Although the respective experimental data are rather scarce, there are some experimental evidences that, in the considered system, the adhesion work and contact angle decrease with increasing pH and decreasing bivalent counterions concentration.[8−10,21] Hence, the adhesion work and contact angle should decrease with increasing velocity U, according to the decrease of the quasi-equilibrium concentrations of cadmium and hydrogen ions near the contact line.

It is important to note that the concentration and potential profiles within the meniscus region are functions of the ratio U/θ rather than the velocity U. As the dynamic contact angle depends on U, the ratio $U/\theta(U)$ is a certain function of U. To find an explicit expression for this function, we have to know the dependence $\theta(U)$.

The concentration polarization becomes stronger as the dynamic contact angle decreases. This means that there is a feed-back in the considered system. The stronger the decrease of quasi-equilibrium concentrations in the meniscus region, the smaller the contact angle that, in turn, leads to a greater decrease of concentrations. Hence, for each velocity U we should have a self-consistent solution which establishes a correspondence between the contact angle and concentrations. However, it is expected that such a solution can exist not for all velocities. With increasing velocity U, the quasi-equilibrium concentrations can become so small that the respective contact angle approaches zero. This happens when the adhesion work decreases to zero and the monolayer does not attach to the substrate surface any more. Therefore, when the velocities are larger than the critical one, the substrate begins to entrain a film of liquid, which forbids the formation of a stable LB coverage.

In some publications, it is assumed that for nonionic monolayers when the ion exchange can be neglected, the wetting dynamics and the critical deposition rate are defined by energy dissipation due to viscous friction and due to molecular processes in the immediate vicinity of the moving contact line.[7,22,23] From the above performed analysis, we can see that in case of charged monolayers the ions redistribution in the solution around the contact line can lead to instability of the system and to interruption of the deposition process. The instability manifests itself in an abrupt increase of the viscous friction caused by a decrease of the contact angle. Therefore, the concentration polarization should have a significant influence on the wetting dynamics and the critical deposition rate.

It is known from experiments that the critical deposition rate decreases with increasing pH and decreasing amount of bivalent counterions in the bulk solution.[21,24,25] In particular, the critical deposition rate is relatively high for arachidic acid monolayers deposited at pH = 2 without any bivalent ions and for the cadmium arachidate monolayer deposited at pH = 6.8 in the presence of 3×10^{-4} M $CdCl_2$ (1.3 and 0.6 cm/s, respectively) but is very small for arachidic acid monolayers in absence of Cd^{2+} ions at pH = 6.8 (smaller than 0.005 cm/s).

Strictly speaking, to establish a correlation between the variation of quasi-equilibrium concentrations and the expected critical velocities, one should know the dependencies $W = W(C^*_{i(eq)})$ and $\theta = \theta_e(C^*_{i(eq)})$. Although such dependencies are not known in details, one can take into account that, for low critical velocities, the decrease of quasi-equilibrium concentrations near the contact line is relatively small. Therefore, for such systems, the quasi-equilibrium concentrations, which correspond to the deposition process disruption, should be of the same order as the bulk concentrations. According to available experimental data, disruption is achieved when the ionic strength is substantially lower than 10^{-6} M (in absence of indifferent electrolytes).

Assuming that the monolayer disruption occurs at the ionic strength of about 10^{-7} M, the diagram presented in Figure 10 gives an estimation of the critical velocity for different subphase compositions. It is seen that the critical velocity should be higher for lower pH and for higher concentrations of bivalent counterions in the bulk solution. As well, the critical velocity rapidly decreases with a decreasing concentration of the potential-determining ions. These findings are in good qualitative agreement with the experimental data discussed above.

The above-described behavior is expected not only for fatty acid but also for other charged monolayers. In particular, the behavior of positively charged monolayers of fatty amines in the presence of bivalent counterions is also in good agreement with the proposed model.[9,21,24,25]

The mechanisms responsible for the experimentally observed decrease of the adhesion work (and contact angle) with increasing in pH and decreasing in bivalent counterions concentration are not completely clear. This effect can be associated with an increase of the monolayer ionization when the concentrations of potential-determining ions decrease what results in increasing repulsion between the charged interfaces.

However, the calculations of electrostatic interaction energy of two arachidic acid monolayers show that its increase with variation of the subphase composition is small and, probably, is not sufficient to explain the observed contact angle decrease. The calculations within the present study show that in the absence of indifferent electrolytes in the subphase, the surface charge density practically does not change with the withdrawal velocity because the actual concentrations of counterions at the interfaces remain almost constant (Figures 5 and 6). Therefore, for such conditions, electrostatic repulsion does not play a significant role.

The situation can change in the presence of small amounts of indifferent electrolytes. The counterions of an indifferent electrolyte are not removed with the deposited film. However, their convective flux is directed toward the contact line because their concentration is larger at the interfaces. In close vicinity of the contact line, this leads to the increase of the quasi-equilibrium concentration of these ions with respect to their bulk concentration.[3] In contrast, near the contact line, the quasi-equilibrium concentrations of potential-determining ions decrease. Therefore, with increasing velocity the counterions of indifferent electrolytes gradually replace the potential-determining ions in the regions around the contact line. The estimations show that, in this case, the surface charge density increases with the velocity, and electrostatic repulsion can additionally complicate the monolayer deposition. As shown in ref 3, the presence of indifferent electrolytes should lead to stronger concentration polarization and smaller critical velocities, which is in agreement with the experimental data.[18,21,24,26] The rigorous studies of the role of indifferent electrolytes in the LB deposition process are currently under way and will be presented later.

It is noteworthy that the approach obtained on the basis of the variable substitution eqs 35 and 36 has a limitation related to the deviations from the condition of local electroneutrality in the virtual solution eq 37 at high rates of the monolayer deposition.[4,5] These deviations can be neglected provided that the following inequality holds (written for the close vicinity of the contact line, where the deviations are most significant):

$$\left|\frac{\rho}{FC}\right| \ll 1 \tag{54}$$

Here, ρ is the bulk charge density, which can be estimated according to the Poisson equation as $\rho = -\epsilon_0\epsilon\Delta\varphi$ by using the obtained solution for the potential distribution. The left-hand side of eq 54 increases fast with the velocity, and for $U/\theta =$ 0.8 cm/s, it takes values of about $1.9\cdot\theta^2$ and $5.7\cdot\theta^2$, respectively, when both R_2M and RM^+ complexes or only R_2M complexes are present. Thus, for sufficiently small contact angles, the condition of eq 54 can be satisfied. For example, with the contact angle $\theta = 5°$ we obtain for the left-hand side of eq 54 about 0.014 and 0.043, respectively, for the two considered cases. However, for the same contact angle $\theta = 5°$, the condition of eq 54 is violated for velocities larger than 0.13 cm/s when both R_2M and RM^+ complexes are present and larger than 0.12 cm/s when only R_2M complexes are present. Probably, deviations from local electroneutrality can also complicate the monolayer deposition.

The concentration polarization near the contact line and meniscus instability can lead to variation of structure and composition of deposited LB films. In particular, according to some observations[27] a stripe structure is formed within the deposited film when a fatty acid monolayer is close to the transition from acid to cadmium salt form (at a pH close to 5.7 in the presence of $\sim 2.5 \times 10^{-4}$ M $CdCl_2$). The stripes are composed from a fatty acid or its cadmium salt. The stripes formation is accompanied by meniscus oscillations. Such behavior can be explained by the periodical change of the critical deposition rate, which is obviously different for the acidic and salt forms of the monolayer.[1]

For strong concentration polarization, the quasi-equilibrium concentration of hydrogen ions can decrease up to 10^{-7} mol/dm^3. For such regimes, the hydroxyl and hydrogen ions produced due to dissociation of water molecules will contribute to the ion balances near the contact line. A similar process, which was called the "water-splitting" effect, is observed in ion-exchange membranes in regimes, when the electric current across the membrane increases above the limiting value.[28−30] In such regimes, a significant part of the current is transferred by ions produced due to the violation of equilibrium of water dissociation. The hydrogen ions, generated near the contact line, can bind to interfacial groups and pass on the substrate with the monolayer. The remaining hydroxyl ions can interact with the counterions transferred from the bulk solution. Therefore, the chemical environment near the contact line can change what should lead to a significant change of the interaction between monolayer and substrate surface. The formation of stripe structures during the deposition can be a consequence of such processes.[1]

The study presented here is based on the assumption that, within the meniscus region, the air/water interface has a quasi-flat geometry. Also, we assumed the contact angle to be sufficiently small. The real shape of the interface is determined by the balance of gravity, capillary, hydrodynamic, and surface forces, and thus, it is much more complex. Using the lubrication approximation (i.e., presenting all variables as functions of the local distance between the interfaces $h(x)$), the results above obtained can be extended for an arbitrary geometry of interface. The assumption of a flat geometry allows one to simplify significantly the integration of equations that describe the system in a general case. At the same time, the physical features of the processes, occurring in close vicinity of the contact line during monolayer deposition, remain the same for any type of geometry. Small contact angles are the most favorable condition for the concentration polarization phenomenon.

As discussed above, for the assumption of a flat geometry of the interface, we have to set the boundary conditions for the quasi-equilibrium concentrations and the potential Φ at a certain finite distance from the contact line, i.e., at $h(x) = l$, to obtain a steady-state problem solution. The calculations were performed for the distance $l = 2$ mm, which is approximately equal to the capillary length $\sqrt{\gamma/\rho g}$. In the regions far from the contact line (where the diffuse layers do not overlap) the quasi-equilibrium concentrations C_i^{qe} and the potential Φ change very slowly with the distance (Figures 5−7). Therefore, the concentrations and potential at the contact line depend only weakly on the choice of the distance l.

One more problem is related to deviations in the concentrations and potential distributions from the local equilibrium in a meniscus cross-section. Such deviations should increase as the flow velocity and distance between the interfaces increase. The estimations show, however, that for moderate deposition rates, these deviations should not be large within the region where the development of concentration polarization can be expected.

7. Conclusions

The deposition of charged Langmuir monolayers to a substrate surface is accompanied by adsorption (binding) of counterions from the subphase, which is necessary for obtaining an electroneutral LB coverage. For the general case, the purely convective transport of ions from the bulk of the subphase toward the three-phase contact line is insufficient to provide the required amount of counterions being withdrawn with the deposited film. Consequently, while the system is approaching to a steady-state regime, ionic concentration profiles are developed in the subphase around the contact line. Moreover, within the region near the contact line (where the diffuse layers overlap), due to the convection produced by the moving interfaces, an additional electric field is induced.

A mathematical model developed in the present study allows one to address the ionic concentration and electric field distributions that are produced around the contact line for different deposition rates up to critical one. The concentration profiles become sharper, and the concentrations in the immediate vicinity of the three-phase contact line can become very small as the deposition rate increases. Substantial changes in the subphase composition result in a decrease of both the adhesion work and the dynamic contact angle. When the deposition rate approaches a critical value, the adhesion work can approach zero, which leads to the disruption of the monolayer deposition. For a given dependence of the adhesion work on the subphase composition, the critical deposition rate can be predicted as a function of the bulk concentrations. Such behavior of the system is in good qualitative agreement with experimental data.

Acknowledgment. Financial assistance by the Bundesministerium für Bildung, Wissenschaft, Forschung und Technologie (BMBF) and Ukrainian Ministry of Education and Science (Joint Project UKR 02/013), and National Ukrainian Academy of Sciences (Project 9-003) is gratefully acknowledged.

References and Notes

(1) Kovalchuk, V. I.; Bondarenko, M. P.; Zholkovskiy, E. K.; Vollhardt, D. *J. Phys. Chem. B* **2003**, *107*, 3486.

(2) Kovalchuk, V. I.; Bondarenko, M. P.; Zholkovskiy, E. K.; Vollhardt, D. *J. Phys. Chem. B* **2004**, *108*, 13449.

(3) Kovalchuk, V. I.; Bondarenko, M. P.; Zholkovskiy, E. K.; Vollhardt, D. *J. Adhes.* **2004**, *80*, 851.
(4) Dukhin, S. S. *Adv. Colloid Interface Sci.* **1993**, *44*, 1.
(5) Shilov, V. N.; Zharkih, N. I.; Borkovskaya, Yu. B. *Colloid J.* **1981**, *43*, 434.
(6) de Gennes, P. G. *Rev. Mod. Phys.* **1985**, *57*, 827.
(7) de Gennes, P. G. *Colloid Polym. Sci*. **1986**, *264*, 463.
(8) Neuman, R. D. *J. Colloid Interface Sci*. **1978**, *63*, 106.
(9) Petrov, J. G.; Angelova, A. *Langmuir* **1992**, *8*, 3109.
(10) Aveyard, R.; Binks, B. P.; Fletcher, P. D. I.; Ye, X. *Colloids Surf., A* **1995**, *94*, 279.
(11) Kjellander, R.; Marchelja, S.; Pashly, R. M.; Quirk, J. P. *J. Phys. Chem. B* **1988**, *92*, 6489.
(12) Kjellander, R.; Marchelja, S.; Pashly, R. M.; Quirk, J. P. *J. Phys. Chem. B* **1990**, *92***,** 4399.
(13) Kovalchuk, V. I.; Bondarenko, M. P.; Zholkovskiy, E. K.; Vollhardt, D. *J. Phys. Chem. B* **2001**, *105*, 9254.
(14) Bodgett, K. B. *J. Am. Chem. Soc*. **1935**, *57*, 1007.
(15) Langmuir, I. *Science* **1938**, *87*, 493.
(16) Ahn, D. J.; Franses, E. I. *J. Chem. Phys.* **1991**, *95*, 8486.
(17) Bloch, J. M.; Yun, W. *Phys. Rev. A* **1990**, *41*, 844.
(18) Hasmonay, H.; Vincent, M.; Dupeyrat, M. *Thin Solid Films* **1980**, *68*, 21.
(19) Johann, R.; Vollhardt, D. *Mater. Sci. Eng., C* **1999**, *8*−*9*, 35.
(20) Gaines, G. L., Jr. *J. Colloid Interface Sci*. **1977**, *59*, 438.
(21) Petrov, J. G.; Kuhn, H.; Möbius, D. *J. Colloid Interface Sci.* **1980**, *73*, 66.
(22) Petrov, P. G. *J. Chem. Soc., Faraday Trans*. **1997**, *93*, 295.
(23) Petrov, J. G.; Petrov, P. G. *Langmuir* **1998**, *14*, 2490.
(24) Petrov, J. G. *Z. Phys. Chem. (Leipzig)* **1985**, *266*, 706.
(25) Petrov, J. G. *Colloids Surf.* **1986**, *17*, 283.
(26) Veale, G.; Peterson, I. R. *J. Colloid Interface Sci.* **1985**, *103*, 178.
(27) Mahnke, J.; Vollhardt, D.; Stöckelhuber, K. W.; Meine, K.; Schulze, H. J. *Langmuir* **1999**, *15*, 8220.
(28) Simons, R. *Electrochim. Acta* **1984**, *29*, 151; **1986**, *31*, 1175.
(29) Zholkovskij, E. K.; Kovalchuk, V. I. *Elektokhimiya* **1988**, *24*, 74 (English translation: *Sov. Electrochem.* **1988**, *24*, 69).
(30) Alcaraz, A.; Ramirez, P.; Mafe, S.; Holdik, H.; Bauer, B. *Polymer* **2000**, *41*, 6627.